ADVANCED ENERGY MATERIALS

www.advenergymat.de

Electrochemical Activity of Hematite Phase in Full-Cell Li-ion Assemblies

Vanchiappan Aravindan and Yun-Sung Lee**

Exploring negative electrodes for high-performance Li-ion power packs and related issues that are hampering their commercialization is a particularly important topic of research. This study investigates the electrochemical activity of low-cost and typical conversion-type hematite (α-Fe_2O_3) anodes in practical assemblies, namely, full-cell configurations. Numerous studies have reported improvements in the electrochemical activity of α-Fe_2O_3 in half cells with Li by tuning the morphology or formulating composites with carbonaceous materials. However, these studies are not sufficient to market them for practical assemblies with conventional cathodes like $LiCoO_2$, $LiMn_2O_4$, $LiFePO_4$ and its derivatives, mainly because of large polarization problems, such as, hysteresis, irreversible capacity loss, volume variation, and capacity fading. Eliminating these issues in the fabrication of full cells is necessary, and this study reviews relevant research activities and discusses future prospects in the field.

1. Introduction

Li-ion batteries (LIBs) are ubiquitous electrochemical energy storage systems used in multifarious applications. Li-ion chemistry is tied to fascinating and favorable features, such as the fact that Li is the lightest metal (equivalent weight $M = 6.94$ g mol^{-1} and specific weight density of 0.534 g cm^{-3}), the most electropositive element (–3.04 V vs. SHE), has a high theoretical capacity (ca. 3862 mA h g^{-1}), high weight and volumetric energy densities, low self-discharge, Li is highly abundant and has no memory effect compared to other equivalent metals such as Na, K, Mg, Ca, and Al.[1,2] In 1990, Sony Inc. introduced the LIB in a so-called "rocking-chair" configuration for consumer applications. This first LIB was composed of graphite as the anode and $LiCoO_2$ as the cathode.[3,4] Intense R&D has led to the exploration of several cathodes, such as layered lithium cobalt oxides ($LiCoO_2$, $Li(CoNiMn)O_2$) or olivine-phase lithium iron phosphates ($LiFePO_4$), which have been developed and commercialized with graphite as the anode, and $LiPF_6$ dissolved in aprotic organic solvents as the electrolyte.[3,5,6] In contrast to the extensive range of cathodes, other negative electrodes exhibiting similar properties to graphite or Li have rarely been commercialized to date. On the other hand, the poor rate capability and subsequent Li-plating of these graphite anodes prevent their practical use in high-power LIBs.[3,5–9] This has inspired the exploration of various kind of intercalation anodes, such as TiO_2 polymorphs, $Li_4Ti_5O_{12}$, $LiTi_2(PO_4)_3$, Nb_2O_5, $TiNb_2O_7$, TiP_2O_7, FeOOH, etc.[10,11] Unfortunately, the reversible capacity (< 250 mA h g^{-1}) and insertion potential of those anodes is too high (> 1.5 V vs. Li), which eventually decreases the net energy density of the full cells. However, an intercalation-type $Li_4Ti_5O_{12}$ anode with a practical energy density of around 200 W h kg^{-1} has reached the commercial market.[4,12] Apart from the intercalation mechanism, sustained Li-storage via conversion and alloy pathways also possible. For instance, Sony exploited Sn-based composites (Sn-Co-Ti-C) as an alloy-type anode in a Nexelion configuration with a mixed cathode.[3,13] However, materials undergoing either conversion or alloying reactions can experience several technical issues including volume variations, large irreversibility, poor inherent electrical conductivity, poor cyclability, and higher working potentials than that of graphite (but lower than those of transition metal oxide-based insertion anodes). Volume variations mainly affect alloying anodes (e.g., Si and Sn), whereas large polarization occurs in conversion-type materials.[14] Intense R&D activities are in full swing to realize such fascinating class materials as prospective anodes for the construction of high-energy and high-power Li-ion power packs. Bearing in mind though that numerous papers and discussions are based on the half-cell performance of the active material.[12,15–18] This report on the other hand details the electrochemical activity/performance of full cells, specifically of α-Fe_2O_3-based full-cell assemblies with various types of cathodes, starting with the conversion reaction.

2. Conversion Reaction

Displacement or conversion is simply stated as a conversion of compound MX_y (where M = Fe, Co, Ni, etc., and

Dr. V. Aravindan
Department of Chemistry
Indian Institute of Science Education and Research (IISER)
Tirupati 517507, India
E-mail: aravindan@iisertirupati.ac.in, aravind_van@yahoo.com
Prof. Y.-S. Lee
Faculty of Applied Chemical Engineering
Chonnam National University
Gwang-ju 500–757, Republic of Korea
E-mail: leeys@chonnam.ac.kr

The ORCID identification number(s) for the author(s) of this article can be found under https://doi.org/10.1002/aenm.201702841.

DOI: 10.1002/aenm.201702841

X = P, S, O, F, Cl, etc.) to the metallic state (M^0) and back to the original state (but not necessarily for all the materials) in a reversible electrochemical reaction.[11,15,19] Generally, this reaction involves the formation of a buffer matrix, such as, Li_2O, Li_2S, Li_3P, LiCl, LiF, etc., alongside the reduction of the metal, which consumes Li-ions in an irreversible manner and causes poor Coulombic efficiency in the first cycle. This redox process involves multiple electron reactions, thus achieving a higher capacity than a graphite anode (>600 mA h g^{-1}) is certainly feasible. Further, the redox potential is generally located at a slightly higher level (>0.5 V vs. Li) than that of graphite, which reduces the risk of Li-plating during high-current operations. Similar to graphite anodes, inevitable electrolyte decomposition occurs in the first cycle and triggers the formation of the solid electrolyte interface (SEI) layer.[20] This SEI layer formation together with the buffer matrix consume Li-ions in an irreversible fashion.

3. Why Fe_2O_3?

The discovery of sustained Li storage in nanoscale metal oxides via conversion pathways led to the extensive investigation of α-Fe_2O_3 as a promising anode for LIB applications. α-Fe_2O_3 has a high theoretical capacity for six-electron reactions (ca. 1008 mA h g^{-1}), high inherent density (5.24 g cm^{-3}), low cost, is easy to prepare, and is environmentally friendly.[11,19,21–24] According to the conversion (or displacement) reaction of α-Fe_2O_3 with Li, the reduction potential is observed at around 0.7 V vs. Li.[15,25] This working potential certainly avoids the risk of Li-plating during high-current operations in contrast to graphite anodes. Nevertheless, among the numerous conversion-type anodes explored are metal oxides, sulfides, chlorides, fluorides, hydroxides,[11,15,26] iron(III) oxide or Fe_2O_3 as an important oxide of iron, as well as FeO and Fe_3O_4. Generally, Fe_2O_3 crystallizes as one of two polymorphs, namely, the predominant rhombohedral α-Fe_2O_3 ore called hematite and the cubic γ-Fe_2O_3, which naturally occurs as maghemite. Different crystalline phases exist, but hematite-phase α-Fe_2O_3 has been predominantly investigated as a negative electrode for LIB applications. Previously, Fe_2O_3 has been extensively studied as an intercalation-type electrode for LIB applications, delivering a reversible capacity reaching 200 mA h g^{-1} at a working potential of around 2.2 V vs. Li.[27–29] Further, Li insertion into α-Fe_2O_3 induces a phase transformation of the oxygen packing in the crystal from a hexagonal close-packed (hcp) structure to a cubic close-packed (ccp) one. Because of the higher insertion potential and large polarization of Fe_2O_3, very few reports have been published on the properties of ferric oxide as an anode.[27] Similar to other metal oxides, particle size is important in determining Li-intercalation chemistry; for example, ultrafine nanosized particulates can accommodate one mole of Li per formula unit ($Li_xFe_2O_3$, $x = 1$) without experiencing a phase change, whereas a small amount of Li-insertion, (0.03 mol) already induces a phase transition from hexagonal to cubic stacking in bulk Fe_2O_3.[27,30,31] Further lithiation of the cubic phase causes the complete destruction of the crystal structure and the subsequent formation of metallic Fe^0 in amorphous Li_2O domains (**Scheme 1**). The overall reaction mechanism can be described as follows in nanoparticles:

$$\alpha\text{-}Fe_2O_3 \rightarrow LiFe_2O_3 \rightarrow Li_2Fe_2O_3 \rightarrow Fe^0 + Li_2O \quad (1)$$

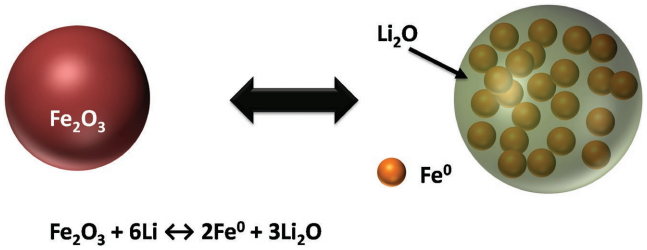

Scheme 1. Schematic representation of the conversion reaction.

Vanchiappan Aravindan is currently working as a Ramanujan Faculty member at the Department of Chemistry of the Indian Institute of Science Education and Research (IISER), Tirupati, India. He received his PhD in 2009 at Gandhigram Rural University, Gandhigram, India. Then he joined the Chonnam National University, Gwang-ju, Korea, as a Post Doctoral Fellow to work with Prof. Yun-Sung Lee. From 2010 until 2017 he was a Senior Scientist at the Energy Research Institute at Nanyang Technological University (ERI@N), Singapore. His research interests include the development of high-performance electrodes and electrolytes for Li-ion chemistry and more.

Yun-Sung Lee is current working as a Full Professor at Chonnam National University, Gwang-ju in Korea. He received his MSc from Chonbuk National University in 1998, where his research work was carried out under the guidance of Prof. Kee-Suk Nahm. He received his Ph.D. in 2001 in Applied Chemistry from Saga University in Japan under the direction of Prof. Masaki Yoshio. He joined the Kanagawa University in Japan in 2001 as a Post-Doctoral Fellow and doctoral researcher with Professor Yuichi Sato. In 2003 he joined Chonnam National University as an Assistant Professor. His research interests lie in the fields of Li-ion batteries, electrode materials, and hybrid capacitor systems.

and in bulk:

$$\alpha\text{-}Fe_2O_3 \rightarrow Li_{0.03}Fe_2O_3 \rightarrow Li_2Fe_2O_3 \rightarrow Fe^0 + Li_2O \quad (2)$$

Irrespective of particle size, Li insertion in α-Fe_2O_3 involves a single-phase reaction followed by a two-phase metallic reduction reaction (Fe^0). However, upon deep discharge, that is, near the reference electrode potential (ca. 5 mV vs. Li) an uptake exceeding the theoretical limit of 6 moles of Li per formula unit occurs. This excess uptake originates from the decomposition of the electrolyte solution and the subsequent formation of a SEI over the active material particulates. However, the inherent characteristics of the amorphous Li_2O matrix promote increased irreversibility. As a result, a very large irreversible capacity loss (ICL) is observed between the first discharge and charge processes. The insulating characteristics of Li_2O affects both the reversibility and the oxidation of Fe^0. This eventually causes the formation of a different charge product than the original one; some groups have reported the formation of FeO[15,32] and others that of γ- or α-Fe_2O_3.[33,34] The overall reaction can be described as follows:

$$Fe^0 + Li_2O \leftrightarrow FeO + 2Li^+ + 2e^- \quad (3)$$

or

$$2Fe^0 + 3Li_2O \leftrightarrow \gamma\text{-or } \alpha\text{-}Fe_2O_3 + 6Li^+ + 6e^- \quad (4)$$

As suggested, the particle size and electrical conductivity in the discharged state (Fe^0 + Li_2O) also influence the formation of the charged product. The reactions depicted in Equation (3) and (4) are highly reversible and continue in subsequent cycles. The Fe^0 nanoparticles gradually increase in size with cycling, which weakens the conductivity of the metallic particles in the presence of the Li_2O matrix. Consequently, rapid capacity fading occurs.[35]

4. Issues and Solutions

Large polarization of the conversion electrodes is a prime issue for conversion-type anodes including α-Fe_2O_3. Large volume variations, higher redox potentials (compared to graphite), poor cyclability and unstable SEI formation are other important issues. In contrast to carbonaceous anodes, the composition of the SEI layer is completely different for conversion anodes. Carbon coating or forming a composite with carbonaceous materials is an efficient way to prevent the agglomeration and growth of active-material particles and thereby to retain the cycling stability and thus enhance the capacity. Using such composites not only improves the cycling stability, but it also leads to a stable SEI formation, and sustains volume variations that occur during electrochemical cycling.[11,16] Further, combining α-Fe_2O_3 with other active materials, such as Sn-C, has also been attempted to resolve these issues.[36,37] In many cases, a reversible capacity exceeding the theoretical value is reported even after the first cycle, obtained by the gradual release of Li^+ trapped within the insulating Li_2O.[21,23,38] The reversible growth of a polymeric gel-like film on the surface of the progressively pulverized anode particles is key in this case.[15,21,23,38] The interface formed between these nanoscale domains facilitates ion transport pathways during the conversion reaction, and allows much Li^+ to be stored. Similar to other conversion-type anodes, α-Fe_2O_3 also suffers from poor cyclability, rate capability, and volume variation issues (>200%) in addition to large first-cycle ICL and polarization. The issues related to the electrochemical performance could be easily addressed by surface modification with conductive coatings or composite formation with carbonaceous materials. However, the ICL and polarization are associated with the inherent properties of the material; they are thus difficult to mitigate completely. Generally, the polarization/hysteresis trend depends on the nature of the anions involved, generally the trend goes: fluorides > oxides > sulfides > nitrides > phosphides > hydrides, which is consistent with Pearson's concept of hard and soft acids and bases.[18,39,40]

While numerous reports have discussed the electrochemical performance of α-Fe_2O_3 with various morphological features and fabricated by different synthesis techniques, these studies were limited to half-cell performances only.[15,17,26] Many good reviews have described the electrochemical activities of hematite in half-cell assemblies.[15,17,26,27,41–43] However, the half-cell performance of a material is insufficient to determine the material's potential as an electrode material in practical LIBs. More importantly, issues of ICL, inherent poor electrical conductivity, and poor stability must be addressed prior to fabricating the full cell. Mitigating ICL has attracted much attention recently; mechanisms for anode pre-treatment, pre-treatment of both cathode and anode, usage of stabilized Li metal powder, chemical lithiation, over-lithiated cathodes, cathodes fabricated with sacrificial salts, spontaneous lithiation, and formulating anodes of Li_3N have been proposed.[44] In the present work, we review the performances of these anodes in practical LIB assemblies only with conventional cathodes.

5. Performance of α-Fe_2O_3 in Full-Cell Assemblies

Hassoun et al.[45] first reported the fabrication of a Li-i(r)on battery with an olivine-phase $LiFePO_4$ cathode. Before full-cell assembly, the $LiFePO_4$ was delithiated to $FePO_4$ and the α-Fe_2O_3 was electrochemically pre-lithiated (Fe^0 + Li_2O) to eliminate ICL issues. In order to be able to better translate the electrochemical profiles, the capacity was limited to 300 mA h g^{-1} and the mass loading was accordingly adjusted to be able to sustain volume variations in the full-cell assembly. Very stable cycling profiles were obtained for this assembly, regardless of the applied current rates. The cell showed a working potential of around 2 V and an energy density of 100 W h kg^{-1}, which was significantly higher in volumetric capacity (1700 Ah L^{-1}) than that of a conventional graphite-based system (760 Ah L^{-1}). Bundles of α-Fe_2O_3 nanorods grown on Ti foil prepared via a hydrothermal approach were previously studied as high-performance anodes for flexible LIBs.[46] Unfortunately, no attempt was made to mitigate any ICL issues, and as a result a dramatic ICL occurred in the first cycle. The full cell, consisting of $LiFePO_4$/α-Fe_2O_3, therefore experienced capacity fading; and the same trend was reflected during the bending experiments as well. Similarly, 3D nanosheets grown over Cu foil showed a

large irreversibility when paired with $LiFePO_4$.[47] The synthesis of polyol-mediated porous α-Fe_2O_3 nanostructures was also explored with commercial $LiFePO_4$.[48] However, electrodes formulated with a 60 wt% loading of active material still suffered from poor cycling stability and large first-cycle irreversibility. Aside from the work by Hassoun et al.,[45] all other attempts were performed by balancing the capacities of individual electrodes obtained by ignoring the first-cycle ICL; dramatic irreversibility was reported irrespective of the hematite nanostructures synthesized. Hariharan et al.[34] pre-heated a cast electrode in Ar atmosphere (up to 300 °C) to ensure the complete melting of the polyvinylidene difluoride (PVDF) binder, which eventually provided better adhesion properties with both conductive carbon and the active material. A somewhat low active material loading of 65 wt% was used to form the electrodes, but they exhibited very high Coulombic efficiencies (ca. 91%) in the first cycle, which is a remarkable value for conversion-type anodes in LIB applications. Because the Coulombic efficiency was high and no pre-treatment was needed to eliminate the ICL, full cells were fabricated with Fe-doped $LiMnPO_4$ ($LiMn_{0.8}Fe_{0.2}PO_4$), which delivered stable capacity profiles for 30 reported cycles. Apart from the environmentally friendly olivine-family cathodes, spinel-phase $LiMn_2O_4$ and its derivatives have also been considered as promising greener cathode materials for high-energy LIB applications. Unfortunately, spinel $LiMn_2O_4$ cannot be paired with carbonaceous anodes because of Mn^{3+} dissolution and subsequent deposition over the carbonaceous surface. Therefore, eliminating Mn^{3+} is an efficient solution to avoid Mn dissolution. Ideally, no Mn^{3+} is present in Ni-doped spinel ($LiNi_{0.5}Mn_{1.5}O_4$), but $Ni^{2+/4+}$ redox reactions do occur beyond the safe operation limit of conventional electrolyte solutions. Excellent battery performances are observed for Ni-doped spinel, but it cannot be paired with carbonaceous counterparts due to the higher redox potential. However, $LiNi_{0.5}Mn_{1.5}O_4$ could be efficiently paired with hematite if the ICL could effectively be mitigated. In this respect, Jayaraman et al.[21] attempted to eliminate the ICL by electrochemically pre-treating electrospun α-Fe_2O_3 nanofibers (**Figure 1**). For this, the α-Fe_2O_3 nanofibers were cycled for two complete cycles in Swagelok fittings before being paired with $LiMn_2O_4$ in a coin-cell assembly. In some cases, the electrolyte solution needed to be topped up. After pre-treatment, the full cell experienced some irreversibility in the first cycle because of the $LiMn_2O_4$ cathode. An exceptional cycle lifetime of 4000 cycles was reported with 70% capacity retention. This was a remarkable cyclability for the hematite phase in the full-cell configuration, regardless of the cathode, morphology, and synthesis procedure. The recycling of waste material is an efficient approach to decrease the cost of raw materials and promote a clean and sustainable system. Mhamane et al.[49] suggested the possibility of using high-yield, high-purity, efficient α-Fe_2O_3 nanostructures from rusted Fe wire waste. Increased capacities were observed for the waste-derived α-Fe_2O_3 upon cycling, regardless of the conductive additive concentration in the half-cell configuration. An irreversibility exceeding 30% was noted in the first cycle for the higher and lower concentrations of the conductive additive. The irreversible capacity could be eliminated though by electrochemically pre-treating the α-Fe_2O_3 with Li in Swagelok fittings and pairing it with a $LiMn_2O_4$ cathode. Unlike in the half cell, some capacitive fading was observed in the full cell, but a 78% retention of the initial reversible capacity was seen after 40 cycles. Aravindan et al.[24] also attempted to mitigate the ICL of α-Fe_2O_3 anodes during the fabrication of full-cell assemblies through three different procedures (**Figure 2**). In the first cell (Cell B), an excess cathode loading was set for compensation; in the second cell (Cell C), the α-Fe_2O_3 nanostructures were electrochemically pre-treated and then paired with the cathode; and in the third cell (Cell A), the cathode was pre-lithiated to over-lithiated spinel ($Li_{1+x}Mn_2O_4$). A large ICL was noted in the first cycle for the anodes in Cell B and Cell A, but the α-Fe_2O_3 nanostructures paired with $Li_{1+x}Mn_2O_4$ (Cell A) delivered a cyclability comparable to that of the electrochemically pre-treated α-Fe_2O_3 anodes (Cell C). One of the main advantages of using an over-lithiated cathode is the reduction in time for the pre-treatment; over-lithiation requires approximately 1 to 3 h, whereas α-Fe_2O_3 anode pre-treatment requires a minimum of two days for the same testing conditions (i.e., same applied current rate). The same group also extended this concept to spinel derivatives, such as $LiNi_{0.5}Mn_{1.5}O_4$ and tavorite-type $LiVPO_4F$ with electrospun α-Fe_2O_3 nanofibers (results unpublished). Decent capacity profiles were noted in both cases; the α-Fe_2O_3 nanofibers in a one-dimensional architecture with the spinel $Li_{1.33}Ni_{0.5}Mn_{1.5}O_4$ cathode and PVDF-hexafluoropropylene as the separator-cum-electrolyte showed a particularly good performance.[50,51] The cell delivered a net energy density of around 193 W h kg^{-1} (based on the total active mass) at a working potential of around 3.27 V.

Veluri and Mitra[52] studied the electrochemical activity of porous α-Fe_2O_3 as an anode with commercial $LiCoO_2$ as the cathode. They formed a composite electrode with 60% active material (α-Fe_2O_3) and 20% each of a conductive additive and a sodium alginate binder. Pre-activation was performed to mitigate the first-cycle ICL. Unfortunately, the full-cell combination ($LiCoO_2$/α-Fe_2O_3) exhibited severe capacity fading upon cycling in a conventional electrolyte solution. However, the inclusion of 2 wt% lithium bis(oxalate)borate (LiBOB) in the electrolyte stabilized the cycling profile. As a result, enhanced cyclability and an energy density of 123 W h kg^{-1} were achieved. Later, Wang et al.[53] measured the electrochemical activity of a free-standing α-Fe_2O_3/graphene/carbon nanotube (CNT) composite anode with a layered $LiCoO_2$ cathode, in which the flexible film contained around 32 wt% of α-Fe_2O_3. Unfortunately, no further details are available for the cell chemistry, including the first charge–discharge characteristics. As noted above, the $LiCoO_2$/α-Fe_2O_3-graphene-CNT cell experienced severe capacity fading in a conventional electrolyte upon cycling. Verrelli et al.[54] suggested Fe doping of high-voltage spinel ($Li_{1.35}Ni_{0.48}Fe_{0.1}Mn_{1.72}O_4$) and pairing it with a meso-carbon microbead (MCMB) artificial graphite/Fe_2O_3 anode. Prior to full-cell fabrication, the MCMB-Fe_2O_3 composite was electrochemically pre-treated in the half-cell assembly with Li. The presence of MCMB in the composite clearly enhanced the Li-storage properties of the hematite phase. As a result, the fabricated 3 V-class LIB cell delivered an energy density of around 300 W h kg^{-1} (based on the cathode mass). The same group extended the procedure to composites of metallic Sn as well (Sn–Fe_2O_3–MCMB in a 4:3:3 ratio)[55] (**Figure 3**). This composite showed all three reaction mechanisms upon testing with

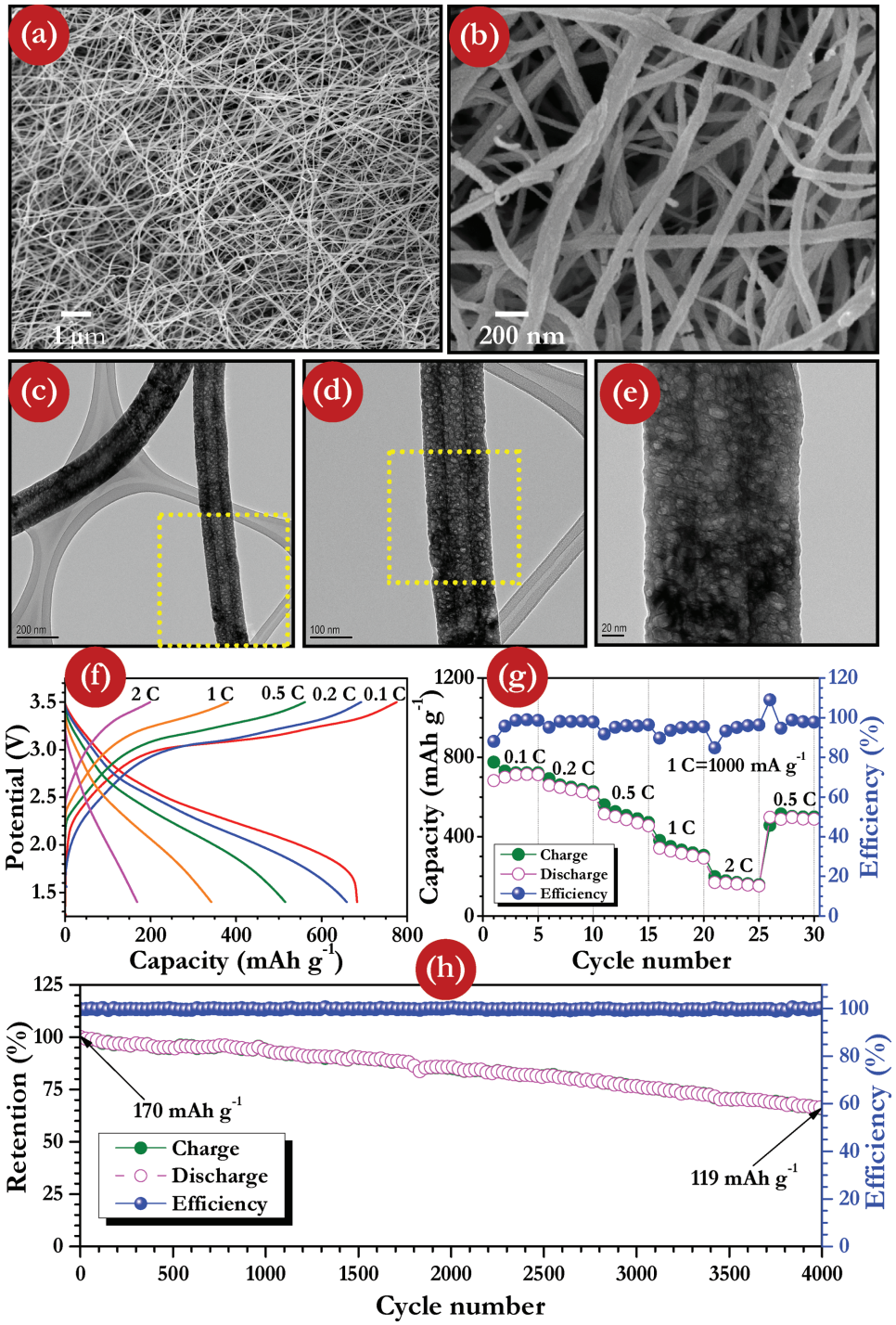

Figure 1. Electrospun porous α-Fe_2O_3 nanofibers: a,b) Field-emission scanning electron microscopy (FE-SEM) images, c–e) transmission electron microscopy (TEM) pictures at different magnifications, f) typical charge–discharge curves of $LiMn_2O_4/\alpha$-Fe_2O_3 (pre-lithiated) cell at various current densities between 1.4–3.5 V, g) rate-capability studies of $LiMn_2O_4/\alpha$-Fe_2O_3 (pre-lithiated) cell with Coulombic efficiency, h) long-term cycling profiles with Coulombic efficiency. Here, 1C is assumed to be 1000 mA g^{-1} with respect to the anode loading. Reproduced with permission.[21] Copyright 2015, Wiley-VCH.

Li in a half-cell configuration: intercalation (MCMB), conversion (Fe_2O_3), and alloying (Sn). After completing 10 galvanostatic cycles with Li, the pre-treated composite anode was paired with high-voltage $LiNi_{0.5}Mn_{1.5}O_4$. A decent cycling profile was obtained for this configuration, with a maximum energy density of around 390 W h kg^{-1}. The composite based on both insertion-, conversion-, and alloying charge-storage materials was additionally modified by replacing the alloy-type material (Sn) with a conversion-type CuO.[37] The ratio was altered slightly to achieve a high-performance anode, with the ratio of CuO/Fe_2O_3

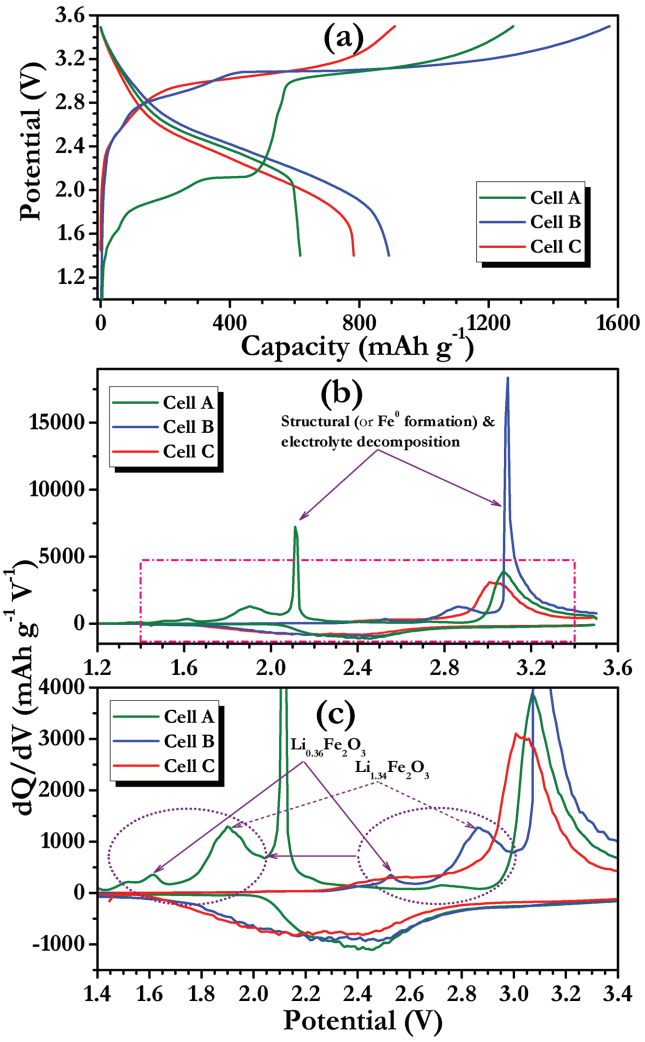

Figure 2. Electrochemical performance of $LiMn_2O_3/\alpha$-Fe_2O_3 full cell at a current density of 100 mA g^{-1}. Capacity and applied currents are based on the anode loading. a) Typical first charge–discharge curves, b) differential capacity profiles of three different kinds of full cells, and c) magnified view of the differential capacity profiles for the marked region. Cell A: Pre-lithiated $Li_{1.26}Mn_2O_4$ cathode is paired with α-Fe_2O_3. Cell B: $LiMn_2O_4/\alpha$-Fe_2O_3 cell is assembled without electrode treatment. Cell C: Pre-treated α-Fe_2O_3 is used to fabricate a full cell with $LiMn_2O_4$. Reproduced with permission.[24] Copyright 2016, Elsevier.

/MCMB fixed at 1:1:2. The final composition contained two conversion-type active materials along with the insertion-type MCMB. A decent reversible capacity exceeding 500 mA h g^{-1} was reported for this anode material. Finally, the full cell was fabricated with the high-voltage spinel $Li_{1.35}Ni_{0.48}Fe_{0.1}Mn_{1.72}O_4$ by pre-cycling the composite anode with metallic Li. The full cell, $Li_{1.35}Ni_{0.48}Fe_{0.1}Mn_{1.72}O_4$/CuO–$Fe_2O_3$–MCMB delivered a maximum energy density of around 400 W h kg^{-1} with excellent cycling stability.

Similar to previous alterations in the composition of the anode, the intercalation-type MCMB could be replaced with non-graphite carbon. The same research group tested the usability of Sn–Fe_2O_3–C as an alloy- and conversion-type anode for practical assembly with the multi-phase olivine

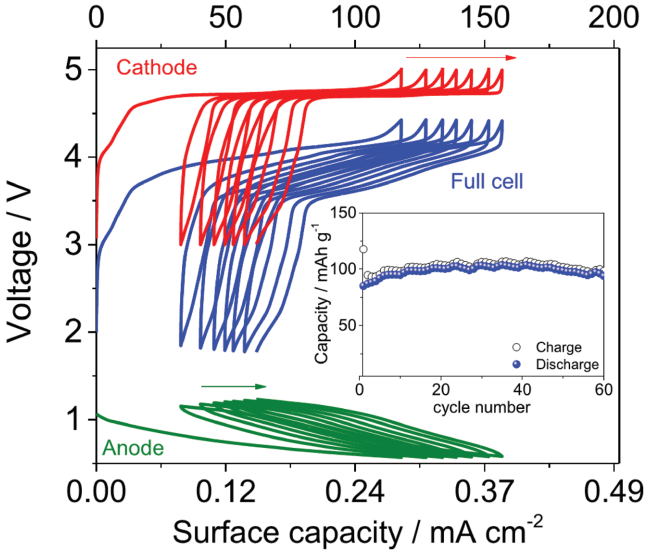

Figure 3. Galvanostatic cycling voltage profiles of the Sn–Fe_2O_3–C/$LiNi_{0.5}Mn_{1.5}O_4$ full cell (blue curve) and of its anodic and cathodic components (green and red curves, respectively). The inset in the figure reports the full-cell cycling behavior. Electrolyte: 1:1 ethylene carbonate–dimethyl carbonate (EC-DMC), $LiPF_6$ (1 M), i.e., LP30. Current density: 50 mA g^{-1}. Theoretical capacity: 148 mA h g^{-1}. Cathode voltage limits: 3–5 V. Room temperature. Reproduced with permission.[55] Copyright 2015, Elsevier.

compound, $LiFe_{0.25}Mn_{0.5}Co_{0.25}PO_4$.[36] The Sn–$Fe_2O_3$–C anode exhibited a reversible capacity exceeding 1000 mA h g^{-1} in the half-cell configuration. In the practical assembly with the $LiFe_{0.25}Mn_{0.5}Co_{0.25}PO_4$ cathode, the cell displayed a maximum energy density of around 300 W h kg^{-1}. Before fabricating the full cell, Sn–Fe_2O_3–C was partially lithiated. An ultra-flexible LIB was also reported using conversion-type Fe_2O_3, in which a flexible substrate was prepared using a composite of PVDF, double-walled CNT, and phenyl-C_{61}-butyric acid methyl ester (PCBM) in a 90:5:5 ratio.[56] As usual, the CNT cones were prepared by chemical vapor deposition (CVD) and transferred to the substrate (**Figure 4**). The cones were decorated with Fe_2O_3 nanocrystals and commercial $LiNi_{0.8}Co_{0.2}O_2$ before employing them as anode and cathode materials, respectively. An enhanced electrochemical activity was noted for the Fe_2O_3-decorated CNT cones compared to the commercial $LiNi_{0.8}Co_{0.2}O_2$-coated ones. Unfortunately, very limited information is available on the cell assembly and elimination of the ICL; a drop of around 48% was reported from the half-cell studies. Rolling and bending of the aforementioned configuration upon cycling was possible, delivering an output of around 120 mA h g^{-1} at a working potential of around 3.1 V. As expected, the full cell was unstable under harsh current testing, but ex situ studies will be performed to ensure the structural integrity of the metal oxide-decorated CNT cones.

6. Outlook

Although several positive features can be noted for conversion-type materials compared to the traditional intercalation materials, the fact that they tend to show a huge irreversibility

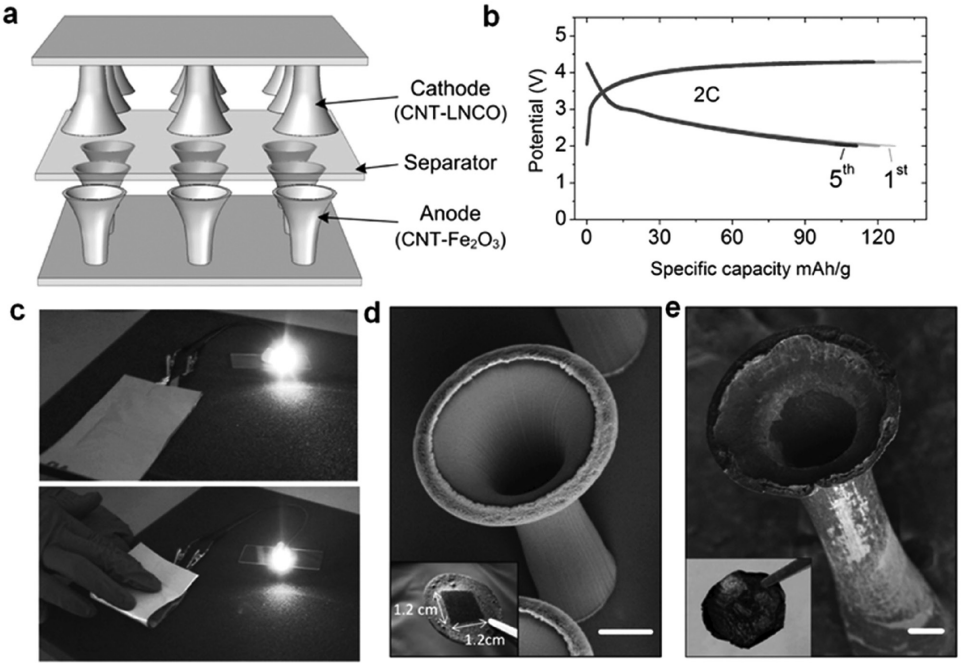

Figure 4. Flexible full cell fabrication and characterizations: a) Schematic representation of the full cell with a CNT cone anode and cathode. b) Charge/discharge curves of full cell: iron oxide–CNT cones and $LiNi_{0.8}Co_{0.2}O_2$ (LNCO)–CNT cones at 2C (first and fifth cycles indicated). c) Flexible CNT cone battery connected to a 3 V white-light LED. d) SEM image of CNT cone, taken at 35° tilt angle, before testing in a full cell. The inset shows a 1.2 cm × 1.2 cm area coverage of transferred CNT cones on the PCBM film. Scale bar: 20 µm. e) SEM image of CNT cone, taken at 40° tilt angle, and picture of the electrode (inset) after 1000 charge/discharge cycles and repeated bending of the electrode. Scale bar: 10 µm. Reproduced with permission.[24] Copyright 2016, Wiley-VCH.

during the first cycle, large volume variation, very high polarization/hysteresis, poor cyclability and unstable SEI formation are still important issues to contend with.[11,15,57] Among the issues stated, the large volume variation and high polarization/hysteresis are associated with the inherent features of the active material, hence these are very difficult to mitigate. However, the remaining issues can be tackled easily by adopting various procedures, such as forming composites with carbonaceous materials, synthesizing the active materials in a hollow-structured morphology, and synthesizing within either active or inactive matrices. These modifications also enable the material to better sustain volume variations observed during the conversion reaction, and hence improved cycle abilities are registered. Moreover, the formation of a composite with conductive additives like carbonaceous components not only provides an improvement in rate capability by enhancing the electronic conductivity, it also stabilizes the SEI formation. Further, it is worth mentioning that carbonaceous materials generally tend to form a more stable layer compared to alloying and conversion-type materials.[20,58–60] In terms of the ICL issue, there are many pre-treating procedures available to eradicate the issue prior to pairing the anodes with cathodes in a full-cell assembly, which we described extensively in our previous review.[57] In contrast to the straightforward procedure of assembling full cells using intercalation materials, conversion- and alloy-based materials desperately require pre-treating procedure, which results in at least one more additional step.[5,7,11,18] The aforementioned issues are not only limited to Fe_2O_3 but are applicable to most conversion- and alloy-type negative electrodes. Therefore, achieving a high-performance configuration that is consistent and has a long duration is a big challenge when using such fascinating anodes in practical assemblies.[14,61–63]

Many reports discuss hematite structures with various morphological features and composite formation with carbonaceous materials as anodes for application in LIBs. Unfortunately, most reports are limited to half-cell studies, which are insufficient to support the use of these materials as practical anodes. The half-cell performance, in other words, the reversible capacity and cyclability of the material, does not necessarily reflect that of full-cell assemblies, regardless of the specific cathode and anode materials in the assembly. Many factors affect full-cell performance when using composite materials as opposed to metallic Li. Li metal is an unlimited source of Li^+ ions, whereas transition metal-based cathodes are restricted. The potential used is critical for cathodes; if the charging potential exceeds a certain limit, Li may plate the anode, whereas structural degradation may occur on the counter side. This is mainly because of the large polarization of the conversion-type anodes; hence, the testing potential window must be selected carefully. This is not the case for half-cell performance tests. In addition, the testing window for conversion-type practical cells is wider, contradictory to those for cells based on either intercalation or alloying mechanisms. This issue holds not just for Fe_2O_3, but for all conversion-mechanism-based anodes. As mentioned earlier, α-Fe_2O_3 structures offer several advantages, including high rate capability, high capacity, and a slightly elevated energy density relative to intercalation-type anodes (except for carbonaceous materials), but polarization hysteresis and volume variation remain critical issues. The ICL is also important, but it can be easily offset by applying scalable techniques such as stabilized Li metal

powder (SLMP) usage, anodic pre-lithiation or pre-treatment, sacrificial salt use, Li_3N blending, and spontaneous lithiation.[44]

Full-cell performances are often studied with α-Fe_2O_3/carbonaceous materials composites either during the synthesis or formation of the electrodes to extend the cyclability, which eventually dilutes the volumetric capacity. However, tuning the composition of a carbonaceous material is among the easiest approaches to continue the development of hematite phase anodes, despite the need for a small reduction in volumetric units. Nevertheless, few reports exist on the long-term cyclability of native α-Fe_2O_3 structures that do not utilize high loads of carbonaceous materials; one example fitting this criterion is an investigation of electrospun α-Fe_2O_3 with $LiMn_2O_4$.[21] Moreover, the cycling stability of electrospun-derived α-Fe_2O_3 nanostructures has been well-established, irrespective of individual morphology.[64] Further, the same group of authors attempted to pair electrospun-derived α-Fe_2O_3 with $LiMn_2O_4$ to eliminate the ICL by adopting three different procedures.[24] Regardless of the procedures, the α-Fe_2O_3 rendered good cycling profiles and compatibility with the spinel cathode, unlike layered oxides. Unfortunately, the higher redox potential of the α-Fe_2O_3 dilutes the net energy density of the 4 V class $LiMn_2O_4$-based system. Therefore, an increase in the energy density is necessary. The same group of authors again explored the possibility of fabricating a one-dimensional LIB using electrospun derived α-Fe_2O_3 nanofibers as the conversion anode and pre-lithiated $Li_{1.33}Ni_{0.5}Mn_{1.5}O_4$ nanofiber as the cathode, in the presence of PVDF-HFP nanofiber membrane as separator-cum-electrolyte.[50] Excellent electrochemical activity was noted for the hematite phase in this fascinating configuration. This clearly suggests that α-Fe_2O_3 displays a good compatibility with spinel cathodes. The development of hematite nanostructures via electrospinning is noteworthy but questionable in scalability, although some start-ups have focused on this system.[65] Furthermore, the adaptation of composites with intercalation and alloying (Sn–MCMB–α-Fe_2O_3) properties is also appealing.[55] Layered $LiCoO_2$ is incompatible with α-Fe_2O_3 in the presence of a conventional electrolyte solution, as clearly demonstrated by two independent reports in the literature.[52,53] A small addition of LiBOB to the conventional solution dramatically enhances the cycling profiles of the system. Such innovations and efforts are necessary to realistically commercialize hematite anodes.

As mentioned, ICL and polarization are issues associated with the inherent properties of the materials. Hence, it is difficult to mitigate these issues completely. However, these issues could be considered negligible when considering their more salient features, such as their high power capability, long-term cycling cyclability, cost-effective nature, and eco-friendliness. A higher cathode loading has also been used to mitigate the ICL and enable a straightforward procedure to fabricate practical assemblies that are similar to those using insertion-type anodes by avoiding pre-treatment procedures. Unfortunately, the dead mass (de-lithiated phase) present on the cathode side dilutes the net energy density of the system and eventually is involved in the unwanted side reaction with the electrolyte. This eventually deteriorates the cell performance upon cycling, which has been made clear by Aravindan et al.[24] In addition to the promising future of hematite anodes in LIBs, hematite may also function as an anode material in high-energy and high-power Li-ion capacitors with activated carbon electrodes.[66–70] However, unfortunately, many works available on α-Fe_2O_3 are limited to half-cell performances only, despite showing substantial enhancements in the electrochemical activity. This is not at all sufficient to bring this fascinating material to the market. Therefore, many more full-cell studies, preferably with spinel cathodes, are needed with consistent performance to realize the development of cost-effective Li-ion power packs with high energy and high power capabilities.

Acknowledgements

V.A. thanks the financial support from the Science & Engineering Research Board (SERB), a statutory body of the Department of Science & Technology, Govt. of India, through the Ramanujan Fellowship (SB/S2/RJN-088/2016). Y.S.L. thank the financial support from National Research Foundation of Korea (NRF) grant funded by the Korea government (Ministry of Science, ICT & Future Planning) 2016R1A4A1012224).

Conflict of Interest

The authors declare no conflict of interest.

Keywords

anodes, batteries, electrochemistry, full cell configuration, lithium ions

Received: October 12, 2017
Revised: November 30, 2017
Published online: January 22, 2018

[1] G. A. Elia, K. Marquardt, K. Hoeppner, S. Fantini, R. Lin, E. Knipping, W. Peters, J.-F. Drillet, S. Passerini, R. Hahn, *Adv. Mater.* **2016**, *28*, 7564.
[2] J. O. Besenhard, M. Winter, *ChemPhysChem* **2002**, *3*, 155.
[3] V. Aravindan, J. Gnanaraj, Y. S. Lee, S. Madhavi, *J. Mater. Chem. A* **2013**, *1*, 3518.
[4] M. M. Thackeray, C. Wolverton, E. D. Isaacs, *Energy Environ. Sci.* **2012**, *5*, 7854.
[5] V. Aravindan, J. Sundaramurthy, P. Suresh Kumar, Y. S. Lee, S. Ramakrishna, S. Madhavi, *Chem. Commun.* **2015**, *51*, 2225.
[6] N.-S. Choi, Z. Chen, S. A. Freunberger, X. Ji, Y.-K. Sun, K. Amine, G. Yushin, L. F. Nazar, J. Cho, P. G. Bruce, *Angew. Chem. Int. Ed.* **2012**, *51*, 9994.
[7] V. Aravindan, Y.-S. Lee, R. Yazami, S. Madhavi, *Mater. Today* **2015**, *18*, 345.
[8] H. D. Yoo, E. Markevich, G. Salitra, D. Sharon, D. Aurbach, *Mater. Today* **2014**, *17*, 110.
[9] J. B. Goodenough, Y. Kim, *Chem. Mater.* **2010**, *22*, 587.
[10] R. Satish, V. Aravindan, W. C. Ling, J. B. Goodenough, S. Madhavi, *Adv. Energy Mater.* **2014**, *4*, 1301715.
[11] V. Aravindan, Y.-S. Lee, S. Madhavi, *Adv. Energy Mater.* **2015**, *5*, 1402225.
[12] B. Zhao, R. Ran, M. Liu, Z. Shao, *Mater. Sci. Eng. R: Reports* **2015**, *98*, 1.
[13] A. K. Shukla, T. Prem Kumar, *Curr. Sci.* **2008**, *94*, 314.
[14] M. R. Palacin, *Chem. Soc. Rev.* **2009**, *38*, 2565.
[15] M. V. Reddy, G. V. Subba Rao, B. V. R. Chowdari, *Chem. Rev.* **2013**, *113*, 5364.
[16] D. S. Su, R. Schlögl, *ChemSusChem* **2010**, *3*, 136.

[17] X. Zheng, J. Li, *Ionics* **2014**, *20*, 1651.
[18] D. Bresser, S. Passerini, B. Scrosati, *Energy Environ. Sci.* **2016**, *9*, 3348.
[19] P. Poizot, S. Laruelle, S. Grugeon, L. Dupont, J. M. Tarascon, *Nature* **2000**, *407*, 496.
[20] E. Peled, S. Menkin, *J. Electrochem. Soc.* **2017**, *164*, A1703.
[21] S. Jayaraman, V. Aravindan, M. Ulaganathan, W. C. Ling, S. Ramakrishna, S. Madhavi, *Adv. Sci.* **2015**, *2*, 1500050.
[22] D. Maiti, V. Aravindan, S. Madhavi, P. Sujatha Devi, *J. Power Sources* **2015**, *276*, 291.
[23] A. Banerjee, V. Aravindan, S. Bhatnagar, D. Mhamane, S. Madhavi, S. Ogale, *Nano Energy* **2013**, *2*, 890.
[24] V. Aravindan, S. Nan, M. Keppeler, S. Madhavi, *Electrochim. Acta* **2016**, *208*, 225.
[25] A. Suryawanshi, V. Aravindan, S. Madhavi, S. Ogale, *ChemSusChem* **2016**, *9*, 2193.
[26] S. Okada, J.-i. Yamaki, *J. Ind. Eng. Chem.* **2004**, *10*, 1104.
[27] M. M. Thackeray, W. I. F. David, J. B. Goodenough, *Mater. Res. Bull.* **1982**, *17*, 785.
[28] S. Komaba, T. Mikumo, N. Yabuuchi, A. Ogata, H. Yoshida, Y. Yamada, *J. Electrochem. Soc.* **2010**, *157*, A60.
[29] A. Manthiram, *Electrochem. Soc. Interface* **2009**, *18*, 44.
[30] D. Larcher, C. Masquelier, D. Bonnin, Y. Chabre, V. Masson, J.-B. Leriche, J.-M. Tarascon, *J. Electrochem. Soc.* **2003**, *150*, A133.
[31] D. Larcher, D. Bonnin, R. Cortes, I. Rivals, L. Personnaz, J.-M. Tarascon, *J. Electrochem. Soc.* **2003**, *150*, A1643.
[32] M. V. Reddy, T. Yu, C. H. Sow, Z. X. Shen, C. T. Lim, G. V. Subba Rao, B. V. R. Chowdari, *Adv. Funct. Mater.* **2007**, *17*, 2792.
[33] S. Hariharan, K. Saravanan, P. Balaya, *Electrochem. Solid State Lett.* **2010**, *13*, A132.
[34] S. Hariharan, V. Ramar, S. P. Joshi, P. Balaya, *RSC Adv.* **2013**, *3*, 6386.
[35] H. Kitaura, K. Takahashi, F. Mizuno, A. Hayashi, K. Tadanaga, M. Tatsumisago, *J. Power Sources* **2008**, *183*, 418.
[36] D. Di Lecce, R. Verrelli, J. Hassoun, *Electrochim. Acta* **2016**, *220*, 384.
[37] D. Di Lecce, R. Verrelli, D. Campanella, V. Marangon, J. Hassoun, *ChemSusChem* **2017**, *10*, 1607.
[38] D. Maiti, V. Aravindan, S. Madhavi, P. S. Devi, *J. Power Sources* **2015**, *276*, 291.
[39] R. G. Pearson, *J. Am. Chem. Soc.* **1963**, *85*, 3533.
[40] R. G. Pearson, *J. Chem. Educ.* **1968**, *45*, 581.
[41] S. Goriparti, E. Miele, F. De Angelis, E. Di Fabrizio, R. Proietti Zaccaria, C. Capiglia, *J. Power Sources* **2014**, *257*, 421.
[42] A. S. Aricò, P. Bruce, B. Scrosati, J. M. Tarascon, W. Van Schalkwijk, *Nat. Mater.* **2005**, *4*, 366.
[43] M. Keppeler, N. Shen, S. Nageswaran, M. Srinivasan, *J. Mater. Chem. A* **2016**, *4*, 18223.
[44] V. Aravindan, Y. S. Lee, S. Madhavi, *Adv. Energy Mater.* **2017**, *7*, 1602607.
[45] J. Hassoun, F. Croce, I. Hong, B. Scrosati, *Electrochem. Commun.* **2011**, *13*, 228.
[46] S. Chen, Y. Xin, Y. Zhou, F. Zhang, Y. Ma, H. Zhou, L. Qi, *J. Mater. Chem. A* **2015**, *3*, 13377.
[47] K. Cao, L. Jiao, H. Liu, Y. Liu, Y. Wang, Z. Guo, H. Yuan, *Adv. Energy Mater.* **2014**, *4*, 1401421.
[48] P. S. Veluri, A. Shaligram, S. Mitra, *J. Power Sources* **2015**, *293*, 213.
[49] D. Mhamane, H.-K. Kim, V. Aravindan, K. C. Roh, M. Srinivasan, K.-B. Kim, *Green Chem.* **2016**, *18*, 1395.
[50] V. Aravindan, N. Arun, N. Shubha, J. Sundaramurthy, S. Madhavi, *Electrochim. Acta* **2016**, *215*, 647.
[51] V. Aravindan, P. Sennu, Y.-S. Lee, S. Madhavi, *J. Phys. Chem. Lett.* **2017**, *8*, 4031.
[52] P. S. Veluri, S. Mitra, *ChemElectroChem* **2017**, *4*, 686.
[53] J. Wang, G. Wang, H. Wang, *Electrochim. Acta* **2015**, *182*, 192.
[54] R. Verrelli, R. Brescia, A. Scarpellini, L. Manna, B. Scrosati, J. Hassoun, *RSC Adv.* **2014**, *4*, 61855.
[55] R. Verrelli, J. Hassoun, *J. Power Sources* **2015**, *299*, 611.
[56] S. Ahmad, D. Copic, C. George, M. De Volder, *Adv. Mater.* **2016**, *28*, 6705.
[57] V. Aravindan, Y.-S. Lee, S. Madhavi, *Adv. Energy Mater.* **2017**, *7*, 1602607.
[58] F. Schipper, D. Aurbach, *Russian J. Electrochem.* **2016**, *52*, 1095.
[59] E. M. Erickson, C. Ghanty, D. Aurbach, *J. Phys. Chem. Lett.* **2014**, *5*, 3313.
[60] S. K. Martha, E. Markevich, V. Burgel, G. Salitra, E. Zinigrad, B. Markovsky, H. Sclar, Z. Pramovich, O. Heik, D. Aurbach, I. Exnar, H. Buqa, T. Drezen, G. Semrau, M. Schmidt, D. Kovacheva, N. Saliyski, *J. Power Sources* **2009**, *189*, 288.
[61] J. Cabana, L. Monconduit, D. Larcher, M. R. Palacín, *Adv. Mater.* **2010**, *22*, E170.
[62] P. Sennu, V. Aravindan, Y.-S. Lee, *Chem. Eng. J.* **2017**, *324*, 26.
[63] A. Chaturvedi, V. Aravindan, P. Hu, R. R. Prabhakar, L. H. Wong, C. Kloc, S. Madhavi, *Appl. Mater. Today* **2016**, *5*, 68.
[64] C. T. Cherian, J. Sundaramurthy, M. Kalaivani, P. Ragupathy, P. S. Kumar, V. Thavasi, M. Reddy, C. H. Sow, S. Mhaisalkar, S. Ramakrishna, *J. Mater. Chem.* **2012**, *22*, 12198.
[65] L. Persano, A. Camposeo, C. Tekmen, D. Pisignano, *Macromol. Mater. Eng.* **2013**, *298*, 504.
[66] V. Aravindan, J. Gnanaraj, Y.-S. Lee, S. Madhavi, *Chem. Rev.* **2014**, *114*, 11619.
[67] A. Brandt, A. Balducci, *Electrochim. Acta* **2013**, *108*, 219.
[68] X. Yu, J. Deng, C. Zhan, R. Lv, Z.-H. Huang, F. Kang, *Electrochim. Acta* **2017**, *228*, 76.
[69] K. Karthikeyan, S. Amaresh, S. N. Lee, V. Aravindan, Y. S. Lee, *Chem. Asian J.* **2014**, *9*, 852.
[70] X. Zhao, C. Johnston, P. S. Grant, *J. Mater. Chem.* **2009**, *19*, 8755.